

Cascade Reactions

Organizing Enzymes on Self-Assembled Protein Cages for Cascade Reactions

Wei Kang⁺, Xiao Ma⁺, Deepika Kakarla, Huawei Zhang, Yunming Fang, Baizhu Chen, Kongfu Zhu, Danni Zheng, Zhiyue Wu, Bo Li,^{*} and Chuang Xue^{*}

Abstract: Cells use self-assembled biomaterials such as lipid membranes or proteinaceous shells to coordinate thousands of reactions that simultaneously take place within crowded spaces. However, mimicking such spatial organization for synthetic applications in engineered systems remains a challenge, resulting in inferior catalytic efficiency. In this work, we show that protein cages as an ideal scaffold to organize enzymes to enhance cascade reactions both in vitro and in living cells. We demonstrate that not only enzyme-enzyme distance but also the improved K_m value contribute to the enhanced reaction rate of cascade reactions. Three sequential enzymes for lycopene biosynthesis have been co-localized on the exterior of the engineered protein cages in *Escherichia coli*, leading to an 8.5-fold increase of lycopene production by streamlining metabolic flux towards its biosynthesis. This versatile system offers a powerful tool to achieve enzyme spatial organization for broad applications in biocatalysis.

Introduction

Self-assembled biomaterials via non-covalent interactions show well-defined structures at both the nanoscales and macroscales with promising functionality and modifiability, thereby enabling a wide range of applications in materials science, bioengineering and medicine.^[1] Particularly, self-assembled protein cage provides a viable template for advanced material synthesis.^[2] Living cells use self-assembled biomaterials to achieve subcellular spatial organization of sequential enzymes to enhance reaction rate and control metabolites flux at branched metabolic nodes, such as membrane-bound organelles, multi-enzyme complexes, protein-bound microcompartment and phase-defined biomolecular condensates.^[3] To this end, protein cages as scaffolds could be leveraged for enzyme spatial organization towards improving catalytic properties.

Enzyme spatial organization has been achieved using self-assembled polymer capsules, liposomes, and micelles.^[4] However, these scaffolds often suffered from heterogeneity, making it difficult to organize enzymes in defined size and shape.^[5] Moreover, these abiotic scaffolds cannot be expressed inside cells. In addition, self-assembled nucleic acids, synthetic protein scaffolds, peptide pairs, and intrinsically disordered regions (IDRs) have been studied for enzyme spatial organization. However, these strategies show various limitations. DNA/RNA-based strategies are hampered by their high cost.^[6] Synthetic protein scaffolds impose adverse effect on protein folding.^[7] IDRs-based enzyme organization occurs only at a specific protein expression level. The enzyme loading capacity of peptide pair-based platform is very low.^[8] Moreover, most of the enzyme assemblies generated by above strategies may dissociate in complex intracellular environments, limiting applications in living cells.

Protein cages, which are self-assembled supramolecular protein nanostructures composed of multiple copies of one (or a few) protein subunits, are being developed as an ideal platform for use in nanotechnology due to their uniformity in size and shape, multiple anchor sites, amenability to chemical and/or genetic modification, and excellent biocompatibility.^[9] However, our attention in this nascent field mainly focuses on biomedical applications such as gene therapy and vaccine.^[10,11] Although there is emerging evidence that protein cages can be used as reaction vessels, however, most of the studies were performed in vitro.^[12] Extending the enzyme organization system from in vitro to in vivo remains challenging due to the different environ-

[*] Prof. W. Kang,⁺ X. Ma,⁺ D. Zheng, Z. Wu, Prof. C. Xue
 State Key Laboratory of Fine Chemicals, Frontiers Science Centre for Smart Materials Oriented Chemical Engineering, School of Bioengineering, Dalian University of Technology
 Dalian 116024 (China)
 E-mail: xue.1@dlut.edu.cn

Prof. W. Kang,⁺ D. Zheng, Prof. C. Xue
 Ningbo Institute of Dalian University of Technology,
 Ningbo 315016 (China)

D. Kakarla, Prof. B. Li
 Department of Mechanical Engineering,
 Kennesaw State University
 GA 0060, Marietta (US)
 E-mail: bli10@kennesaw.edu

Prof. H. Zhang, K. Zhu
 Department of Biomedical Engineering,
 Southern University of Science and Technology
 Shenzhen 518055 (China)

Prof. Y. Fang
 National Energy Research Centre for Biorefinery,
 Beijing University of Chemical Technology,
 Beijing 100029 (China)

Prof. B. Chen
 School of Biomedical Engineering,
 SUN YAT-SEN University
 Shenzhen 518000 (China)

[†] These authors contributed equally to this work.

ments between test tubes and cellular milieu. However, biosynthesis in living cells features ease of scale up and low cost. Recently, rod-like virus-like particles (VLPs) have been explored for in vivo enzyme organization.^[13] However, linearly arranged self-assembled protein scaffolds are known to interfere with cell division, limiting their applications for in vivo enzyme organization.^[13b] In addition, globularly organized enzymes are more widely found in nature (e.g., metabolon and multienzyme complexes). Thus, there is a compelling need to develop a biomimetic enzyme organization strategy.

Here, we show that Mi3, a globular protein cage, can serve as an ideal scaffold to organize multiple enzymes spatially both in vitro and in living cells, leading to enhanced biosynthesis (Figure 1a). First, we show that different enzymes with different shapes and sizes can be targeted to the Mi3 surface in high copy numbers. Using enzymes in menaquinone biosynthesis as a model system, we find that the enzyme-enzyme distance and enzyme kinetics both contribute to the enhanced reaction rate of assembled cascade reaction. Prokaryote was once thought of “bag of enzymes” lack of membrane-based spatial organization.

Using MBP and fluorescent proteins as model cargo proteins, we demonstrate that proteins can be attached to the surface of Mi3 spontaneously not only in vitro but also inside living *E. coli* with complex intracellular environments, endowing prokaryotes with spatial organization. Finally, we showed that organizing sequential enzymes on Mi3 protein cages can streamline the metabolic flux, leading to an 8.5-fold increase in lycopene synthesis in engineered *E. coli*.

Results and Discussion

Design, Synthesis, and Characterization of Protein Cage Directed Multienzyme Assemblies

We began by assembling tri-enzyme (MenF, MenD and MenH) on Mi3 to construct multi-enzyme assemblies for 2-succinyl-6-hydroxy-2,4-cyclohexadiene-1-carboxylate (SHCHC) synthesis, which catalyzes the first three reactions for menaquinone biosynthesis (Figure 1b). Previously, we have shown that the complexed menaquinone biosynthetic enzymes can affect the catalytic reaction rate.^[14] Mi3 is an

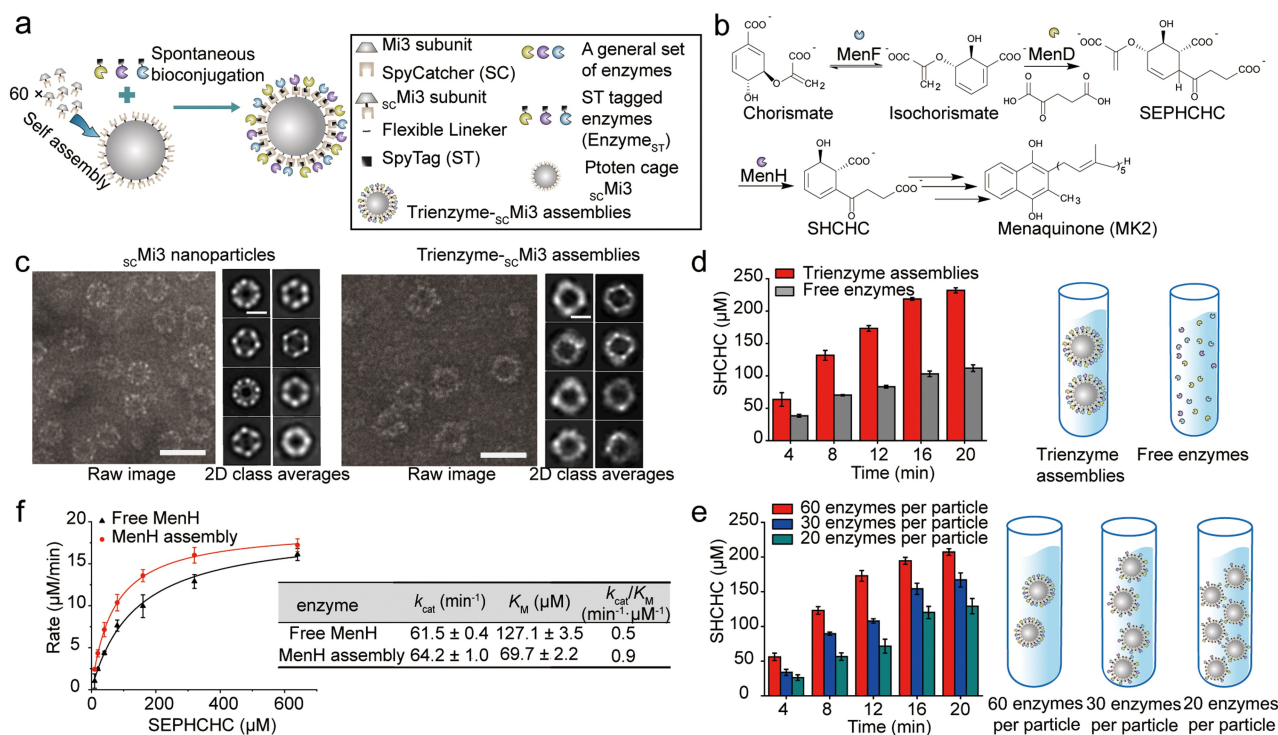


Figure 1. Design, synthesis, and characterization of protein cage directed multienzyme assemblies of sequential enzymes. a) Schematic illustration of synthetic multienzyme assemblies based on SpyCatcher-Mi3 (sc Mi3) protein cage. b) MenF, MenD, and MenH catalyzed cascade reaction. c) Negatively stained transmission electron microscope (TEM) images and 2D class averages of sc Mi3 protein cages (left) and trienzyme assemblies of MenF_{ST}/MenD_{ST}/MenH_{ST- sc Mi3} (right) showing intact and monodisperse nanoparticles. In 2D class averages of trienzyme assemblies, the originally clear edge of sc Mi3 protein cage was surrounded by a fluffy seam of electron-density, which corresponds to the attached enzymes. Scale bars, 50 nm (raw images) and 20 nm (2D class averages). d) Comparison of SHCHC production of “free” enzyme system and tri-enzyme assembly system. e) Comparison of SHCHC production between three tri-enzyme assembly systems with different enzyme densities. Schematic illustrations of the reaction systems are shown on the right panels of 1d and 1e, respectively. f) MenH assembly exhibited enhanced enzyme kinetics. The kinetic curves were fitted to the Michaelis–Menten equation with R^2 values > 0.99, giving k_{cat} and K_M reported in the right table. The total amounts of the enzymes, the initial concentrations of substrate, and the volumes of the reaction mixtures were kept the same in 1d, 1e, and 1f, respectively. Error bars indicate the standard deviations of three independent experiments in 1d, 1e and 1f.

engineered dodecahedral protein cage based on the aldolase of thermophilic bacteria,^[15] consisting of 60 copies of identical subunit with a diameter of 26 nm.^[16] SpyTag/SpyCatcher (ST/SC) is a site-specific protein reactive pair linked by intermolecular isopeptide bond.^[17] ST-containing enzymes and SC-containing protein cage (both are separated by (GGGS)₃ linker) were expressed and purified to homogeneity (Figure S1). To construct protein cage scaffolded multienzyme assemblies, sequential enzymes (MenF_{ST}, MenD_{ST} and MenH_{ST}) were mixed with SC-containing Mi3 (scMi3) at room temperature in 50 mM Tris buffer (pH 7.6) for 1 hour. While MenF and MenH are monomers,^[18] MenD tends to form oligomers.^[19] Multimeric enzymes may bind to multiple protein cages to form enzyme agglomerates. We found that when enzymes are molar excess (i.e., MenF_{ST}:MenD_{ST}:MenH_{ST}:scMi3 = 3:3:3:1), tri-enzyme assemblies are monodisperse particles (Figure S2). In comparison, decreasing the ratio of enzymes to protein cage (i.e., MenF_{ST}:MenD_{ST}:MenH_{ST}:scMi3 = 1:1:1:3) leads to the formation of enzyme agglomerates (Figure S2). For better characterization of protein cage-based enzyme assemblies, we used molar excess enzymes to yield monodisperse nanoparticles in the following studies.

The protein cage scaffolded enzyme assemblies were further characterized using size exclusion chromatography (SEC), dynamic light scattering (DLS), and transmission electron microscope (TEM). SEC purification of the tri-enzyme assemblies and following SDS-PAGE analysis of the collected peaks showed no unconjugated scMi3 (Figure S3), indicating high loading capacity of scMi3 nanoparticle, which can be attributed to the large gap between attachment sites (≈ 5 nm, Figure S4) and the flexible linkers (GGGS)₃ in the fusion enzymes. The maximum number of conjugated enzymes per scMi3 nanoparticle is ≈ 60 . DLS showed that scMi3 exhibits a hydrodynamic diameter of 28.4 ± 2.5 nm whereas scMi3-scaffolded tri-enzyme assembly is 38.0 ± 3.4 nm (Figure S5). TEM analysis of both scMi3 nanoparticles and tri-enzyme assemblies show monodisperse particles (Figure 1c) with the diameter of scMi3 at 25.9 ± 0.7 nm (average of 100 particles) and tri-enzyme assemblies at 31.8 ± 0.8 nm (average of 100 particles), which also show the successful assembly of MenF_{ST}, MenD_{ST}, and MenH_{ST} on the surface of scMi3. The 2D average images show clear edges of “naked” scMi3 nanoparticles and blurred edges of tri-enzyme assemblies (Figure 1c). The blurred edges of tri-enzyme assemblies may be due to the motion of attached enzymes incurred by the (GGGS)₃ flexible linker. 2D single-particle image of scMi3 matches I3-01 protein cage (related to Mi3 protein cage) crystal structure^[20] whereas tri-enzyme assemblies exhibit an additional electron-dense layer (Figure S6). Characterization of single enzyme assemblies showed similar results by SEC, DLS and TEM (Figure S7). Together, these results demonstrate that Mi3 successfully organized sequential enzymes on its surface.

To briefly explore the performance of protein cage organized sequential enzymes on the reaction rate of the cascade reaction, we prepared Mi3 scaffolded tri-enzyme assemblies of MenF, MenD and MenH. In general, we found a higher production rate of SHCHC, compared to the “free”

enzyme system (Figure 1d). Orchestrating metabolic pathways in living organisms is often achieved by altering the spatial organization of sequential enzymes.^[21, 22] It has been reported that the distance between assembled enzymes is crucial for facilitated intermediate transport and enhanced reaction rates.^[14a, 23] We thus compared three different enzyme systems with different spatial enzyme organizations (Figure 1e). Given the fact that the Mi3 is a dodecahedral nanoparticle, the average enzyme-enzyme distances are calculated to be 4.6 nm, 7.4 nm and 9.2 nm for the three systems, respectively (Figure S8). Therefore, the “60 enzymes per nanoparticle” system with the highest enzyme density yields the shortest enzyme-enzyme distance, thereby resulting in the highest production rate of SHCHC, followed by “30 enzymes per nanoparticle” and “20 enzymes per nanoparticle” (Figure 1e). To understand the underlying mechanism of the enhanced reaction rate, we explored the enzymatic kinetics of the assembled enzymes. MenF is known to catalyze a reversible reaction. In addition, because the product (SEPHCHC) of MenD is not visible in UV/Vis range, we chose MenH catalyzed reaction for kinetics analysis. Two reaction groups were established: (1) MenH_{ST} and scMi3 (MenH assemblies); (2) MenH_{ST} and Mi3 (free MenH). Despite the similar apparent k_{cat} values, the apparent K_M value for MenH assemblies was 46 % lower than that of “free” MenH (Figure 1f, 69.7 vs 127.1 μ M). We speculate that a preferred microenvironment, an increased local enzyme concentration, and/or a favorable orientation towards substrate may contribute to the decreased K_M . It has been proposed that the improved enzyme kinetics contribute to the increased reaction rate of colocalized enzymes.^[24] Our study shows that the enhanced reaction rate of tri-enzyme assemblies is entailed by a combination of spatial organization induced close proximity and improved enzyme kinetics.

scMi3-Scaffolded Protein Spatial Organization in Living Cells

To the best of our knowledge, Mi3 has not been used inside living cells to organize proteins intracellularly. We first assembled model cargo proteins, maltose binding protein (MBP) and cyan fluorescent protein (CFP), on scMi3 cages in living *E. coli*. To this end, ST-containing MBP (MBP_{ST}), ST-containing CFP (His-tagged CFP, His-CFP_{ST}), and scMi3 were co-expressed in *E. coli* (Strain Immu1) using two compatible plasmids (Figure 2a). Similarly, strain Immu0 expressing scMi3, MBP and His-tagged CFP was made to serve as a control. The spontaneous bioconjugation in living cells between scMi3 and ST-containing proteins was confirmed by western blot and SDS-PAGE (Figure 2b and Figure S9). Intact and spherical scMi3 cages as well as scMi3-scaffolded protein assemblies (scMi3-CFP/MBP) were visualized by thin-section TEM (Figure 2c). Naked scMi3 in control strain Immu0 has a mean diameter of 50.7 nm whereas the mean diameter of scMi3-CFP/MBP protein assemblies was increased to 79.0 nm (Figure 2d). The diameter of scMi3 cages embedded in ultrathin section is larger than purified samples, because the high-pressure

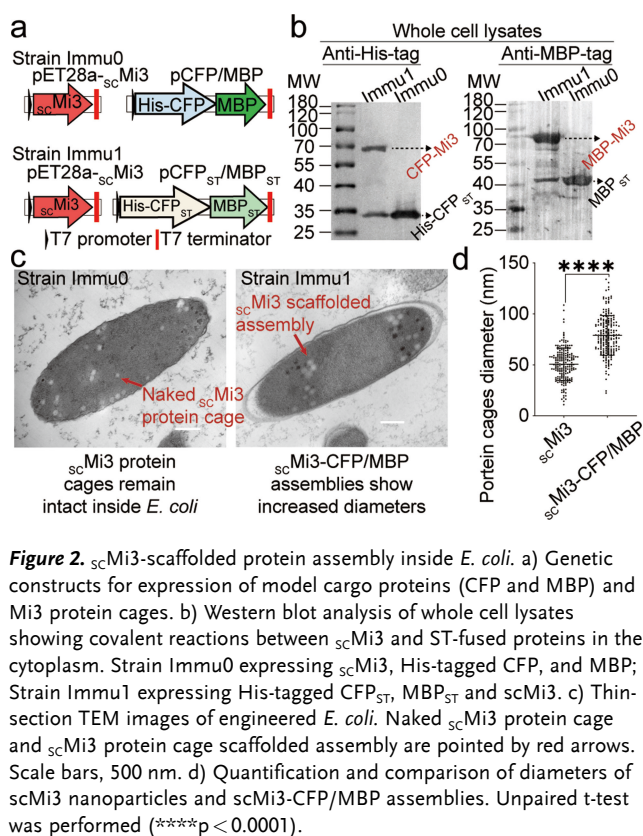


Figure 2. $scMi3$ -scaffolded protein assembly inside *E. coli*. a) Genetic constructs for expression of model cargo proteins (CFP and MBP) and $scMi3$ protein cages. b) Western blot analysis of whole cell lysates showing covalent reactions between $scMi3$ and ST-fused proteins in the cytoplasm. Strain Immu0 expressing $scMi3$, His-tagged CFP, and MBP; Strain Immu1 expressing His-tagged CFP_{ST}, MBP_{ST} and $scMi3$. c) Thin-section TEM images of engineered *E. coli*. Naked $scMi3$ protein cage and $scMi3$ protein cage scaffolded assembly are pointed by red arrows. Scale bars, 500 nm. d) Quantification and comparison of diameters of $scMi3$ nanoparticles and $scMi3$ -CFP/MBP assemblies. Unpaired t-test was performed (**** $p < 0.0001$).

freezing, chemicals fixation and plastic embedding process changed the original volume of protein cages. The increased diameter of protein assemblies indicates the successful attachment of ST-containing proteins on the surface of protein cages. In addition, by monitoring of cell growth we found that expression of $scMi3$ and formation of protein cages have no adverse effect on cell growth, indicative of the biocompatibility of $scMi3$ protein cage to *E. coli* (Figure S10).

To further demonstrate that $scMi3$ can direct protein self-assembly inside cells, we performed fluorescence lifetime imaging microscopy (FLIM) by assembling a pair of fluorescent proteins in the living *E. coli* (Figure 3a), CFP and YFP (yellow fluorescent protein). CFP_{ST}, YFP_{ST}, and $scMi3$ were co-expressed inside *E. coli* (Strain Fluo1) to enable $scMi3$ scaffolded assembly of fluorescent proteins. A corresponding control strain without the ability to mediate the attachment of fluorescent proteins (Strain Fluo0) was also made. Fluo1 exhibited a significantly decreased fluorescence lifetime of the CFP signal than that of Fluo0 (Figure 3b, 1192.9 vs. 1962.4 ps), suggesting a fluorescence resonance energy transfer (FRET) due to the proximity of CFP and YFP in Fluo1 via $scMi3$ mediated colocalization. Notably, the distance between CFP_{ST} and YFP_{ST} on the surface of $scMi3$ was calculated to be 5.4 nm according to the FRET efficiency, consistent with the theoretical calculation. In addition, protein organization on protein cage enables distinct fluorescent patterns. Specifically, fluorescence microscopy images reveal that both CFP and YFP signals are evenly distributed throughout the cytosol in Fluo0

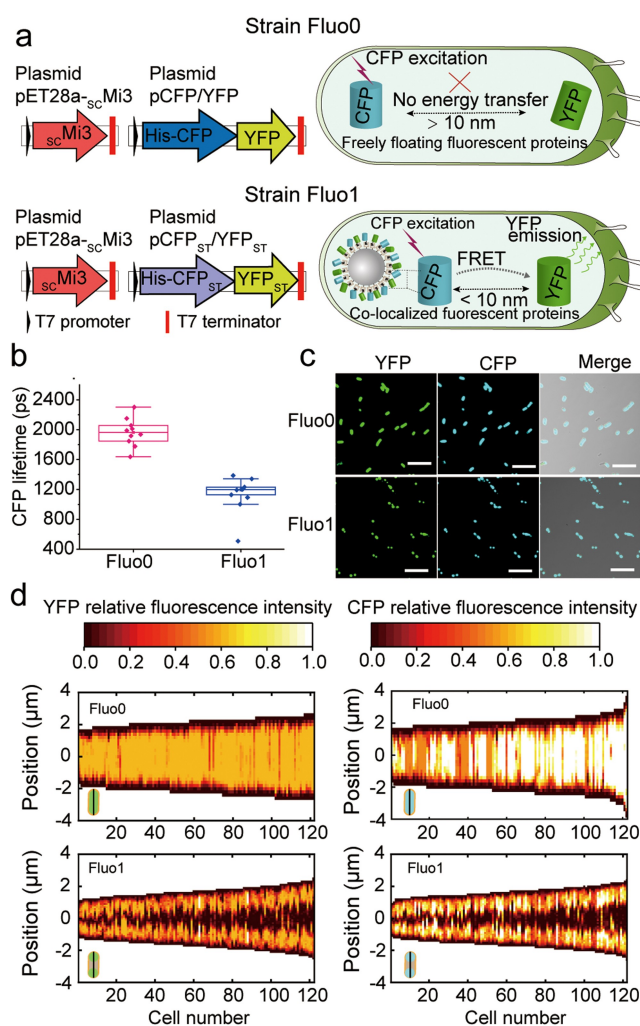


Figure 3. $scMi3$ -scaffolded assembly of fluorescent proteins in *E. coli*. a) Schematic illustration of genetic constructs for expression of fluorescent proteins and $scMi3$ protein cages. Strain Fluo0 (control strain) expressing CFP, YFP, and $scMi3$. Strain Fluo1 expressing CFP_{ST}, YFP_{ST} and $scMi3$. b) Measurement of CFP lifetime of the engineered *E. coli* by FLIM. Error bars indicate the standard deviations of ten replicates. CFP and YFP were brought into close proximity after colocalization as evidenced by shortened fluorescence lifetime of donor fluorescent protein CFP. c) Confocal images of the two engineered *E. coli* strains showing distinctive fluorescent signals. Scale bars, 10 μm . d) Localization patterns of YFP and CFP shown in (c) were quantified, respectively. Vertical heatmaps representing intensities of fluorescent protein across the long cell axis were generated using microbeJ. Demographs show the fluorescent intensity across a population of cells arranged by cell length. Uniform fluorescence was observed in strain Fluo0. In contrast, fluorescence was concentrated at the poles of Fluo1.

whereas the fluorescent signals are concentrated at the poles of Fluo1 (Figure 3c and 3d). Thus, it is possible to functionally separate cytoplasm into distinct areas using protein cage-based protein self-assembly. Altogether, these results show that $scMi3$ protein cages can serve as scaffolds for colocalization of different ST-containing proteins in living *E. coli*.

Spatial Organization of Enzymes Enable Increased Lycopene Production inside *E. coli*.

Cells use spatial organization to orchestrate multiple reactions with high efficiency. As a proof of concept, we extended $_{sc}Mi3$ -scaffold to colocalize three key enzymes in lycopene biosynthesis in living *E. coli*. Two pathways are required to realize heterologous production of lycopene in *E. coli* (Figure 4a). The mevalonate pathway (MVP) is

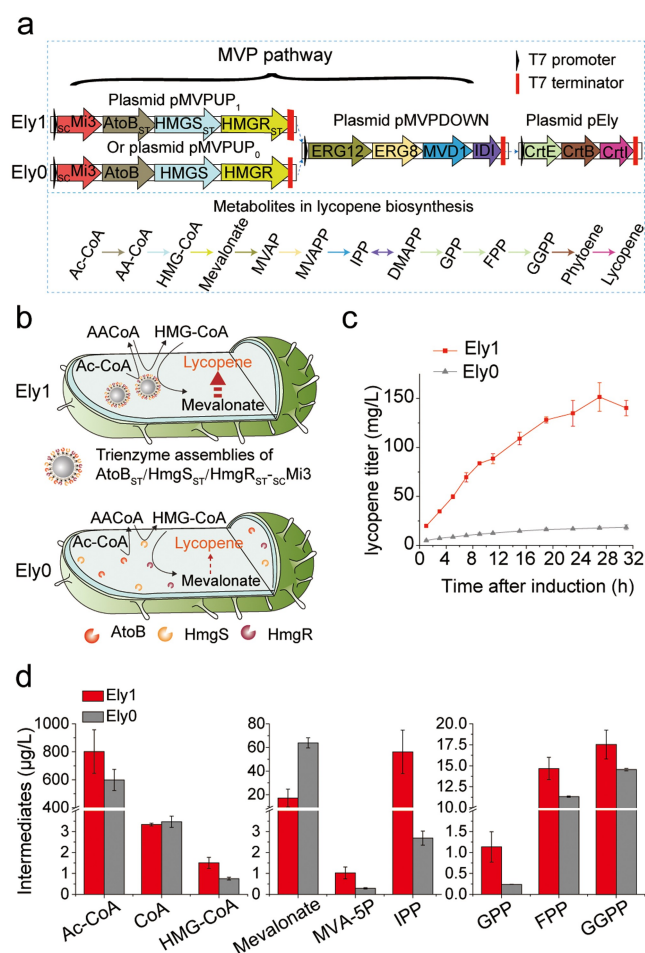


Figure 4. Synthetic tri-enzyme assemblies increase lycopene production in living *E. coli*. a) Genetic constructs of the engineered strains for lycopene biosynthesis. ERG12, mevalonate kinase; ERG8, phosphomevalonate kinase; MVD1, mevalonate diphosphate decarboxylase; IDI, isopentenyl pyrophosphate isomerase; CrtB, phytoene synthase; CrtI, phytoene desaturase; Ac-CoA, acetyl-CoA; AA-CoA, acetoacetyl-CoA; HMG-CoA, hydroxymethylglutaryl-CoA; MVAP, mevalonate-5-phosphate; MVAPP, mevalonate pyrophosphate. b) Tri-enzyme assemblies of AtoB_{ST}/HmgS_{ST}/HmgR_{ST- $_{sc}Mi3$} in strain Ely1 are expected to enhance lycopene production through streamlining the metabolic flux. Strain Ely0 expressing freely floating enzymes serves as the control. c) Comparison of the lycopene titers between the two engineered strains showing enhanced lycopene biosynthesis in strain Ely1. d) Mass spectrometry-based quantification of key intermediates at 24 hours after induction showing that synthetic multienzyme complex can promote the metabolic flux towards lycopene biosynthesis. Error bars indicate the standard deviations of three independent experiments.

responsible for the supply of C₅ building blocks, isopentenyl pyrophosphate (IPP) and its allylic isomer dimethylallyl pyrophosphate (DMAPP), which both are universal precursors for terpene biosynthesis. Then the isoprenoid diphosphates synthase (CrtE) carries out a continuous head-to-tail condensation of the C₅ building blocks to give isoprenoid precursors including geranyl diphosphate (GPP, C₁₀), farnesyl diphosphate (FPP, C₁₅), and geranylgeranyl diphosphate (GGPP, C₂₀). The following enzymes of CrtB and CrtI are responsible for the modification of GGPP to generate lycopene. It has been proven that the sufficient supply of IPP and DMAPP is critical for efficient terpene biosynthesis,^[25] and synthetic multienzyme complexes of HmgR, AtoB and HmgS enhance the production of terpene.^[8, 26] To this end, we assembled HmgR, AtoB and HmgS on the surface of $_{sc}Mi3$ in *E. coli*. ST was fused to the N or C terminus of enzyme, yielding fusion enzymes of HmgR_{ST}, AtoB_{ST}, and HmgS_{ST}, respectively. To facilitate verification of these enzymes, three immunogenic tags, Flag-tag, His-tag, and S-tag, were added to HmgS_{ST}, HmgR_{ST}, and AtoB_{ST}, respectively. Three compatible plasmids (pMVPUP₁/pMVPUP₀, pMVPDown, and pEly) containing all the genes of MVP pathway and lycopene biosynthetic enzymes were made and then co-transformed into *E. coli* (Figure 4a).

Two strains were constructed: Ely1 (strain contains synthetic multienzyme assemblies) and control strain Ely0 (strain only contains “free” enzymes, Figure 4b). Strain Ely1 expresses three ST-fused enzymes and $_{sc}Mi3$, which allows the spontaneous attachment of the three ST-fused enzymes onto the exterior of $_{sc}Mi3$ protein cages, resulting in tri-enzyme assemblies of AtoB_{ST}/HmgS_{ST}/HmgR_{ST- $_{sc}Mi3$} . Ely0 is the control strain; the only difference between Ely1 and Ely0 is the absence of the ST in AtoB, HmgS and HmgR in Ely0 (Figure 4a). Western blot analysis confirmed that ST-containing enzymes were successfully coupled to the $_{sc}Mi3$ (Figure S11). Unconjugated ST-containing enzymes were also observed in strain Ely1, indicating that not all ST-containing enzymes were conjugated to $_{sc}Mi3$. The incomplete assembly is likely due to the different expression levels of the $_{sc}Mi3$ and the ST-fused enzymes. In contrast, no bands corresponding to the conjugated adducts were observed in reference strain Ely0 (Figure S11). Above results confirmed that the successful attachment of ST-fused enzymes on $_{sc}Mi3$ in living cells.

In tandem, we compared the lycopene production between Ely1 and Ely0 in shake-flask fermentations. Both strains were cultivated under the same condition and induced by IPTG at the same OD₆₀₀ value. Lycopene was extracted from the cell pellets by using acetone, and then quantified from calibration curve of the standard lycopene using HPLC (Figure 4c and Figure S12). Lycopene started to be accumulated after induction in both strains. Strikingly, the titer of lycopene reached 151.6 mg L⁻¹ in strain Ely1 at 27 h, which was 8.5-fold of that in Ely0 (17.8 mg L⁻¹). This result is consistent with previous reports that the assembly of the three enzymes can increase product yields.^[8, 26] To confirm that the increased lycopene production was not a result of enzyme stabilization induced by the fusion of

(GGGS)₃-ST, we constructed strain Ely0' harboring ST-fused enzymes and Mi3, which does not form synthetic multienzyme assemblies. Strain Ely0' expressing Mi3, HmgR_{ST}, AtoB_{ST}, and HmgS_{ST} showed similar lycopene titer compared to that of strain Ely0 (Figure S13). To exclude the possibility that different enzyme expression levels lead to the varied lycopene production, proteomic analysis was performed to quantify the protein abundance in engineered strains. Ely0, Ely0', and Ely1 exhibited similar protein expression levels of lycopene producing enzymes (Figure S14). This result indicates that the increased lycopene production is due to the enzyme assembly. Intriguingly, only a modest ≈2-fold increase of SHCHC was observed in vitro whereas a dramatic ≈8.5-fold increase of lycopene was observed inside cells. We speculate that the lower diffusion coefficient in living cells contributes to the much more significant enhancement in lycopene production. It is well recognized that the bacterial cytoplasm is highly crowded and the high viscosity can slower the diffusion of metabolites. The tri-enzyme assemblies of AtoB_{ST}/HmgS_{ST}/HmgR_{ST}-_{SC}Mi3 can overcome this diffusion barrier and promote the metabolic flux, leading to significant improvement of lycopene production.

We also monitored the levels of key metabolites of lycopene production in vivo over time (Figure 4d and Figure S15). Although, Ely1 and Ely0 showed similar levels of MVP pathway's substrate (acetyl-CoA, Ac-CoA), the overall metabolic flux towards lycopene biosynthesis was promoted in Ely1 compared with Ely0 as evidenced by the increased levels of most of the MVP pathway's intermediates. For example, the isoprenoid precursors, GPP, FPP, and GGPP, for lycopene biosynthesis, were 4.7-fold, 29.6%, and 20.7% higher in Ely1 (GPP 1.136 μg L⁻¹, FPP 14.673 μg L⁻¹, GGPP 17.549 μg L⁻¹) than those of Ely0 (GPP 0.239 μg L⁻¹, FPP 13.319 μg L⁻¹, GGPP 14.544 μg L⁻¹) at 24 hours after induction. It is known that Ac-CoA is also the universal precursor for native *E. coli* metabolism. Thus, this result suggests that formation of tri-enzyme assemblies can streamline the metabolic flux and compete more substrate for lycopene biosynthesis. However, it is unclear why less mevalonate is accumulated in Ely1. We reconstituted the three-enzyme (AtoB, HmgS, and HmgR) catalyzed reaction in vitro, which converts Ac-CoA to mevalonate (Figure S16). We found that the tri-enzyme assemblies system showed higher level of mevalonate production (0.0171 mg L⁻¹) than that of "free" enzyme system (0.0110 mg L⁻¹) at six minutes after reaction initiation (Figure S16). This result indicates that colocalization of AtoB, HmgS, and HmgR, streamlines the metabolic flux, and thus leads to the increased production of mevalonate in vitro. We speculated that the consumption of mevalonate as well as the downstream reactions is accelerated in Ely1 in vivo by mechanisms such as the enzyme self-assembly mediated alteration of spatial organization of the cytoplasm, and/or nonspecific binding of downstream enzymes with the protein cage-based multienzyme assemblies, leading to less buildup of mevalonate in Ely1 in vivo.

To confirm that increased lycopene production is due to self-assembled tri-enzyme assemblies, we investigated the

effect of substrate concentration on the cascade reaction using reconstituted mevalonate production in vitro. All systems contained the same enzyme composition but different substrate concentrations (80 mg L⁻¹ substrate, 400 mg L⁻¹ substrate, and 2000 mg L⁻¹ substrate, Figure S17). While tri-enzyme assemblies with 80 mg L⁻¹ substrate showed a significant increase of mevalonate production compared with the "free" enzyme system (59.2% increase), tri-enzyme assemblies with 2000 mg L⁻¹ and 400 mg L⁻¹ substrate only generated slight increases compared to "free" enzyme system (19.7% and 14.1% increase, respectively). We found that the fold increase of mevalonate is reversibly proportional to substrate concentration (Figure S17). We speculate that the moderate increase of mevalonate production in systems with higher substrate concentration (400 mg L⁻¹ and 2000 mg L⁻¹) is because that higher substrate concentration provides relatively sufficient reactants for cascade reaction, such that colocalization of sequential enzymes on the protein cage which facilitates intermediates transfer could not greatly enhance the cascade reactions. In comparison, tri-enzyme assemblies can provide catalytic benefits when the reactants supply is the limiting factor of the cascade reaction (i.e., the substrate level is low) by facilitating the intermediate transfer. This phenomenon is particularly interesting since many of the substrates for the value-added products, especially the substrates belonging to the secondary metabolisms, the substrates at the branched point of metabolism, as well as the substrate for the heterologous biosynthesized products, are kept in a relatively low level in the host organisms, leading to a low level of desired products. Our study shows that enzyme spatial organization can potentially solve this issue. Taken together, the global changes of the metabolic intermediates are consistent with the speculation that the enzyme spatial organization increases the supply of precursors for terpenoid biosynthesis.

To evaluate the contribution of facilitated intermediate transfer to enhanced reaction rate, we compared the tri-enzyme system with a di-enzyme system both in vitro and in vivo. For the di-enzyme assembly system, the second enzyme of the cascade reaction remains freely floating and is not included in the enzyme assembly. For the lycopene production in *E. coli*, three groups were explored: (1) Ely1 containing tri-enzyme assemblies of AtoB_{ST}, HmgS_{ST} and HmgR_{ST}; (2) Ely0 containing freely floating enzymes; (3) Ely2 containing di-enzyme assemblies of AtoB_{ST} and HmgR_{ST}. The only difference between Ely1 and Ely2 is that the second enzyme of the cascade reaction, HmgS, is not fused with ST (Figure 5a) in Ely2 and thus cannot be coupled to the surface of protein cages. The level of lycopene production was in the following order: Free enzyme system < Di-enzyme assemblies < Tri-enzyme assemblies (Figure 5b). Although both of the enzyme assembly systems (Ely1 and Ely2) showed higher levels of lycopene production, the tri-enzyme assembly strains are much more productive. Specifically, after 30 h of shake-flask fermentation revealed that the Ely1 showed titers about 4.5-fold higher than that of the Ely2 and 6.4-fold higher than that of the free enzyme strain Ely0. We also compared the tri-enzyme system with di-enzyme system for SHCHC

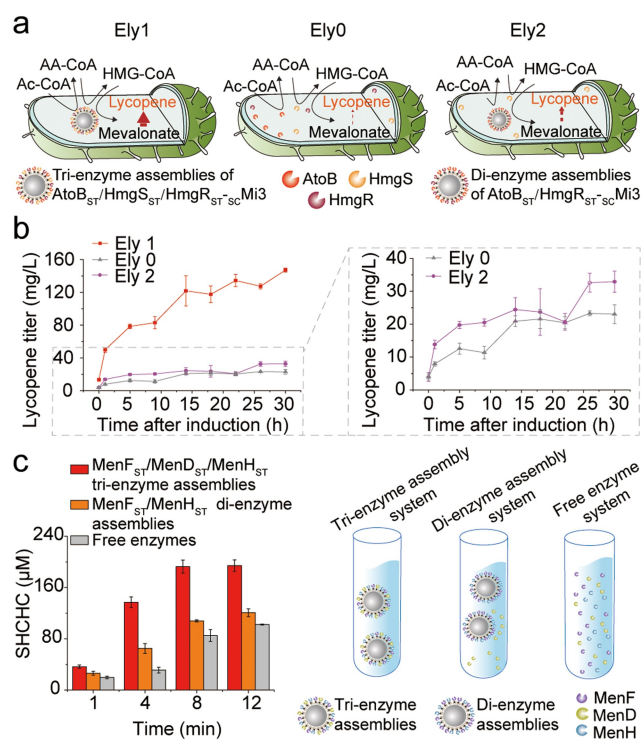


Figure 5. Comparison of reaction rate of cascade reaction between tri-enzyme assemblies and di-enzyme assemblies. a) Schematic of experimental setup for lycopene production in vivo. Ely1 contains tri-enzyme assemblies of AtoB_{ST}, HmgS_{ST} and HmgR_{ST-sc}; Ely0 is the control strain containing only freely floating enzymes; Ely2 contains di-enzyme assemblies of AtoB_{ST} and HmgR_{ST-sc} and the second enzyme for this cascade reaction, HmgS without ST, remains freely floating. b) Ely1 containing tri-enzyme assemblies is much more productive compared to Ely0 and Ely2 in vivo. Ely2 only shows a moderate increase of lycopene production than that of Ely0. c) Tri-enzyme assemblies of MenF, MenD, and MenH exhibits the highest level of SHCHC production in vitro compared to the di-enzyme assembly system and “free” enzyme system. Di-enzyme assemblies only show a moderate increase of SHCHC production than that of “free” enzyme system in vitro. Error bars indicate the standard deviations of three independent experiments in 5 b and 5 c.

production in vitro. As shown in Figure 5c, tri-enzyme assemblies showed a significantly higher level of SHCHC production than that of di-enzyme assemblies and free enzymes. In all the tested in vitro and in vivo systems, the tri-enzyme assembly systems showed a pronounced increase of product whereas di-enzyme assembly systems only exhibited a moderate product increase. We interpret that the absence of the second enzyme in the di-assemblies breaks the streamlined metabolic flux. Other mechanisms, such as enhanced enzyme kinetics (as evidenced by MenH assemblies relative to “free MenH”, Figure 1f), steric hindrance for the inhibitor’s binding (for the in vivo system), or preferred orientation after attachment to the protein cage, may contribute to the moderate enhancement of di-enzyme assemblies. Overall, these results indicate that organizing enzymes on protein cages can facilitate intermediate transfer and enable enhanced cascade reactions.

Conclusion

In this work, we developed a versatile strategy for organizing enzymes on protein cages (i.e., Mi3) for enhanced biocatalysis. Model proteins and enzymes with different sizes and shapes were successfully attached to the surface of protein cage _{sc}Mi3 with high density through ST/SC chemistry not only in vitro but also inside living cells. In vitro, the purified tri-enzyme assemblies in menaquinone biosynthesis appear to be monodisperse and homogeneous nanoparticles with improved catalytic properties. The enhanced reaction rate after enzyme spatial organization was attributed to the enforced proximity and improved enzyme kinetics. Inside *E. coli*, the engineered strain expressing self-assembled AtoB_{ST}-HmgS_{ST}-HmgR_{ST-sc}Mi3 tri-enzyme assemblies shows an 8.5-fold increase of lycopene production in comparison to the reference strain only expressing freely floating lycopene biosynthetic enzymes. Overall, this work shows globular protein cage can serve as an ideal scaffold for constructing tailor-made multienzyme assemblies for a wide range of applications in synthetic biology and metabolic engineering. We envision that enzyme spatial organization provides a potent tool to improve the performance of engineered pathways in host cells, which is orthogonal to traditional strategies of synthetic biology. In addition, our studies also demonstrate protein cage can not only be used in extracellular applications but also holds great potential in intracellular applications through in situ protein spatial organization.

Acknowledgements

Financial support for this work was provided via the National Key Research and Development Program (no. 2021YFC2103703), the National Natural Science Foundation (no. 22178046), Kennesaw State University Graduate College Funding, the Youth program of National Natural Science Foundation (no. 21807043 and no. 31900046), and the Fundamental Research Fundamental Funds for the Central Universities (no. DUT20RC(3)069 and no. DUT22-LAB601). We thank Dr. Huihui Wan for mass spectrometry analysis.

Conflict of Interest

The authors declare no conflict of interest.

Data Availability Statement

The data that support the findings of this study are available on request from the corresponding author. The data are not publicly available due to privacy or ethical restrictions.

Keywords: Cascade Reactions · Enzymes · Protein Cages · Self-Assembly

- [1] a) N. Stephanopoulos, J. H. Ortony, S. I. Stupp, *Acta Mater.* **2013**, *61*, 912–930; b) R. Freeman, M. Han, Z. Álvarez, A. Lewis Jacob, R. Wester James, N. Stephanopoulos, T. McCleendon Mark, C. Lynsky, M. Godbe Jacqueline, H. Sangji, E. Luijten, I. Stupp Samuel, *Science* **2018**, *362*, 808–813.
- [2] a) B. Li, N. You, Y. Liang, Q. Zhang, W. Zhang, M. Chen, X. Pang, *Energy Environ. Mater.* **2019**, *2*, 38–54; b) C. Mao, J. Solis Daniel, D. Reiss Brian, T. Kottmann Stephen, Y. Swee-ney Rozamond, A. Hayhurst, G. Georgiou, B. Iverson, M. Belcher Angela, *Science* **2004**, *303*, 213–217.
- [3] C. Greening, T. Lithgow, *Nat. Rev. Microbiol.* **2020**, *18*, 677–689.
- [4] A. Küchler, M. Yoshimoto, S. Luginbühl, F. Mavelli, P. Walde, *Nat. Nanotechnol.* **2016**, *11*, 409–420.
- [5] B. J. Johnson, W. Russ Algar, A. P. Malanoski, M. G. Ancona, I. L. Medintz, *Nano Today* **2014**, *9*, 102–131.
- [6] a) W. P. Klein, R. P. Thomsen, K. B. Turner, S. A. Walper, J. Vranish, J. Kjems, M. G. Ancona, I. L. Medintz, *ACS Nano* **2019**, *13*, 13677–13689; b) R. P. Chen, D. Blackstock, Q. Sun, W. Chen, *Nat. Chem.* **2018**, *10*, 474–481.
- [7] F. Jia, B. Narasimhan, S. Mallapragada, *Biotechnol. Bioeng.* **2014**, *111*, 209–222.
- [8] J. E. Dueber, G. C. Wu, G. R. Malmirchegini, T. S. Moon, C. J. Petzold, A. V. Ullal, K. L. J. Prather, J. D. Keasling, *Nat. Biotechnol.* **2009**, *27*, 753–759.
- [9] W. M. Aumiller, M. Uchida, T. Douglas, *Chem. Soc. Rev.* **2018**, *47*, 3433–3469.
- [10] I. Lostalé-Seijo, J. Montenegro, *Nat. Chem. Rev.* **2018**, *2*, 258–277.
- [11] S. Nooraei, H. Bahrulolum, Z. S. Hoseini, C. Katalani, A. Hajizade, A. J. Easton, G. Ahmadian, *J. Nanobiotechnol.* **2021**, *19*, 59.
- [12] a) S. Tetter, D. Hilvert, *Angew. Chem. Int. Ed.* **2017**, *56*, 14933–14936; *Angew. Chem.* **2017**, *129*, 15129–15132; b) P. C. Jordan, D. P. Patterson, K. N. Saboda, E. J. Edwards, H. M. Miettinen, G. Basu, M. C. Thielges, T. Douglas, *Nat. Chem.* **2016**, *8*, 179–185; c) D. P. Patterson, B. Schwarz, R. S. Waters, T. Gedeon, T. Douglas, *ACS Chem. Biol.* **2014**, *9*, 359–365.
- [13] a) Q. Wei, S. He, J. Qu, J. Xia, *Bioconjugate Chem.* **2020**, *31*, 2413–2420; b) M. J. Lee, J. Mantell, L. Hodgson, D. Alibhai, J. M. Fletcher, I. R. Brown, S. Frank, W. F. Xue, P. Verkade, D. N. Woolfson, M. J. Warren, *Nat. Chem. Biol.* **2018**, *14*, 142–147.
- [14] a) W. Kang, J. Liu, J. Wang, Y. Nie, Z. Guo, J. Xia, *Bioconjugate Chem.* **2014**, *25*, 1387–94; b) W. Kang, T. Ma, M. Liu, J. Qu, Z. Liu, H. Zhang, B. Shi, S. Fu, J. Ma, L. T. F. Lai, S. He, J. Qu, S. Wing-Ngor Au, B. Ho Kang, W. C. Yu Lau, Z. Deng, J. Xia, T. Liu, *Nat. Commun.* **2019**, *10*, 4248.
- [15] Y. Hsia, J. B. Bale, S. Gonen, D. Shi, W. Sheffler, K. K. Fong, U. Nattermann, C. Xu, P.-S. Huang, R. Ravichandran, S. Yi, T. N. Davis, T. Gonen, N. P. King, D. Baker, *Nature* **2016**, *535*, 136–139.
- [16] a) K. D. Brune, D. B. Leneghan, I. J. Brian, A. S. Ishizuka, M. F. Bachmann, S. J. Draper, S. Biswas, M. Howarth, *Sci. Rep.* **2016**, *6*, 19234; b) T. U. J. Bruun, A. C. Andersson, S. J. Draper, M. Howarth, *ACS Nano* **2018**, *12*, 8855–8866.
- [17] B. Zakeri, J. O. Fierer, E. Celik, E. C. Chittock, U. Schwarz-Linek, V. T. Moy, M. Howarth, *Proc. Natl. Acad. Sci. USA* **2012**, *109*, E690–E697.
- [18] a) J. M. Johnston, M. Jiang, Z. Guo, E. N. Baker, *PLoS One* **2013**, *8*, e61325; b) S. Kolappan, J. Zwahlen, R. Zhou, J. J. Truglio, P. J. Tonge, C. Kisker, *Biochemistry* **2007**, *46*, 946–953.
- [19] A. Dawson, P. K. Fyfe, W. N. Hunter, *J. Mol. Biol.* **2008**, *384*, 1353–1368.
- [20] J. Votteler, C. Ogohara, S. Yi, Y. Hsia, U. Nattermann, D. M. Belnap, N. P. King, W. I. Sundquist, *Nature* **2016**, *540*, 292–295.
- [21] J. B. French, S. A. Jones, H. Deng, A. M. Pedley, D. Kim, C. Y. Chan, H. Hu, R. J. Pugh, H. Zhao, Y. Zhang, T. J. Huang, Y. Fang, X. Zhuang, S. J. Benkovic, *Science* **2016**, *351*, 733–737.
- [22] T. Laursen, J. Borch, C. Knudsen, K. Bavishi, F. Torta, H. J. Martens, D. Silvestro, N. S. Hatzakis, M. R. Wenk, T. R. Dafforn, C. E. Olsen, M. S. Motawia, B. Hamberger, B. L. Moller, J. E. Bassard, *Science* **2016**, *354*, 890–893.
- [23] a) J. Fu, M. Liu, Y. Liu, N. W. Woodbury, H. Yan, *J. Am. Chem. Soc.* **2012**, *134*, 5516–9; b) J. Fu, Y. R. Yang, A. Johnson-Buck, M. Liu, Y. Liu, N. G. Walter, N. W. Woodbury, H. Yan, *Nat. Nanotechnol.* **2014**, *9*, 531–536.
- [24] L. J. Sweetlove, A. R. Fernie, *Nat. Commun.* **2018**, *9*, 2136.
- [25] a) K. W. George, M. G. Thompson, J. Kim, E. E. K. Baidoo, G. Wang, V. T. Benites, C. J. Petzold, L. J. G. Chan, S. Yilmaz, P. Turhanen, P. D. Adams, J. D. Keasling, T. S. Lee, *Metab. Eng.* **2018**, *47*, 60–72; b) V. J. Martin, D. J. Pitera, S. T. Withers, J. D. Newman, J. D. Keasling, *Nat. Biotechnol.* **2003**, *21*, 796–802.
- [26] J. Qu, S. Cao, Q. Wei, H. Zhang, R. Wang, W. Kang, T. Ma, L. Zhang, T. Liu, S. Wing-Ngor Au, F. Sun, J. Xia, *ACS Nano* **2019**, *13*, 9895–9906.

Manuscript received: September 21, 2022

Accepted manuscript online: October 26, 2022

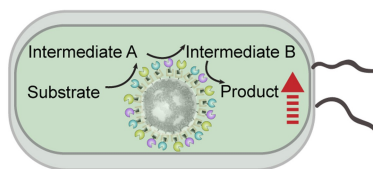
Version of record online: ■■■, ■■■



Research Articles

Cascade Reactions

W. Kang, X. Ma, D. Kakarla, H. Zhang,
Y. Fang, B. Chen, K. Zhu, D. Zheng, Z. Wu,
B. Li,* C. Xue* **e202214001**

Organizing Enzymes on Self-Assembled
Protein Cages for Cascade Reactions



 Protein cage subunit
 Sequential enzymes

Self-assembled protein cages enabled
spatial organization of prokaryotes

Self-assembled protein cages were functionalized to achieve spatial organization of sequential enzymes in living cells, which confer cascade reactions with optimal local concentrations and micro-environment, thereby entailing enhanced biocatalytic performance.